

Did Uranus' regular moons form via a rocky giant impactor?

Jason Man Yin Woo¹, Christian Reinhardt¹, Marco Cilibarsi^{1,2}, Alice Chau¹, Ravit Helled¹, Joachim Stadel¹

¹Institute for Computational Science, University of Zürich, Winterthurerstrasse 190, 8057 Zürich, Switzerland

²Department of Physics, ETH Zurich, Wolfgang-Pauli-Strasse 27, 8093 Zürich, Switzerland

Abstract

The formation of Uranus' regular moons has been suggested to be linked to the origin of its enormous spin axial tilt ($\sim 98^\circ$). A giant impact between proto-Uranus and a $2-3 M_{\text{Earth}}$ impactor could lead to a large tilt and to the formation of a debris disc, where prograde and circular satellites are accreted. The most intriguing features of the current regular Uranian satellite system is that it possesses a positive trend in the mass-distance distribution and likely also in the bulk density, implying that viscous spreading of the debris disc after the giant impact plays a crucial role in shaping the architecture of the final system. In this paper, we investigate the formation of Uranus' satellites by combining results of SPH simulations for the giant impact, a 1D semi-analytic disc model for viscous spreading of the post-impact debris disc, and N-body simulations for the assembly of satellites from a disc of moonlets. Assuming the condensed rock (i.e., silicate) remains small and available to stick onto the relatively rapid growing condensed water-ice, we find that the best case in reproducing the observed mass and bulk composition of Uranus' satellite system is a pure-rocky impactor with $3 M_{\text{Earth}}$ colliding with the young Uranus with an impact parameter $b = 0.75$. Such an oblique collision could also naturally explain Uranus' large tilt and possibly, its low internal heat flux. The giant impact scenario can naturally explain the key features of Uranus and its regular moons. We therefore suggest that the Uranian satellite system formed as a result of an impact rather than from a circumplanetary disc. Our results also suggest that objects beyond the water snow-line could be dominated by rocky objects similar to Pluto and Triton. Future missions to Uranus and its satellite system would further constrain the properties of Uranus and its moons and provide further insight on their formation processes.

1. Introduction

The gas giants Jupiter and Saturn are thought to form their regular satellites from a circumplanetary disc which is generated from gas and dust directly accreted from the protoplanetary disc (e.g. Canup and Ward, 2006; Mosqueira and Estrada, 2003) during the formation of the gas giants. While a similar scenario has also been proposed for the formation of the satellite systems of the less massive ice giants (Canup and Ward, 2006; Szulágyi et al., 2018), it is currently still unclear whether Uranus and Neptune can acquire a circumplanetary disc during their formation since these planets are not expected to undergo runaway gas accretion (Helled et al., 2020 and references therein).

Uranus has a remarkable spin-axial tilt of $\sim 98^\circ$ relative to its orbital plane. It has been hypothesised that Uranus' large obliquity was caused by a giant impact late in its formation (e.g. Safronov, 1966; Slattery et al., 1992). Recent high-resolution smoothed particle hydrodynamics (SPH) simulations show that such a late giant impact can not only explain Uranus' current axial tilt, spin rate, and low thermal flux (Fortney et al., 2011; Nettelmann et al., 2013; Pearl and Conrath, 1991), but also to deposit enough debris into a circumplanetary orbit after the collision that can lead to the formation of its regular satellites system (Kegerreis et al., 2018; Kurosaki and Inutsuka, 2018; Reinhardt et al., 2020).

There are five regular satellites of Uranus with prograde and nearly circular orbits: Miranda, Ariel, Umbriel, Titania and Oberon, from the closest to farthest. Their masses range from $\sim 10^{-6}$ to $\sim 10^{-4} M_{\text{U}}$ and their total masses are $1.05 \times 10^{-4} M_{\text{U}}$, where $M_{\text{U}} = 8.7 \times 10^{25} \text{ kg}$ is Uranus' mass. An intriguing feature of the Uranian satellite system is the positive trend of the mass-distance distribution, in which the innermost Miranda is an order of magnitude less massive than the intermediate Ariel and Umbriel; and the outermost Titania and Oberon are the most massive. Recent N-body simulations have failed to obtain such a positive trend of the mass-distance distribution with the initial conditions following the non-spattered impact generated disc, which are very compact in the innermost region, right after the giant impact (Ishizawa et al., 2019).

To overcome this problem, Ishizawa et al. (2019) suggested that the thermal and viscous spreading of the impact debris disc must be considered in order to explain the positive trend of the mass-distance distribution. These two effects were hence included in a later study on the Uranian satellite formation (Ida et al. 2020). Ida et al. (2020) successfully reproduced the positive trend of the mass-distance distribution by the combination of a 1D viscous diffusion equation (Hartmann et al., 1998) and analytical models for dust condensation and evolution. According to their analytical solution, more ice (in this study, we refer to water ice only unless specified) condensed in the outer region as the disc spreads and cools, leaving the inner disc depleted in water ice as water vapour is lost to Uranus when the disc spreads. As a result, the surface density of the condensed ice has a positive gradient which can explain the more massive satellites in the outer region.

In addition to the positive trend of the mass-distance distribution, another peculiar feature of the Uranian satellite system is that the satellites are thought to be composed of roughly half rock and half ice, with the innermost satellite Miranda being the most icy one (Jacobson et al., 1992). So far no studies have attempted to combine impact simulation results with viscous spreading of the impact generated disc to explain the bulk composition of the Uranian satellites. Ida et al. (2020) suggest that their model can explain the roughly 1 to 1 rock-to-ice ratio of the satellites, although they considered only the icy component of the disc, since early condensed silicate particles remain small and could potentially stick to later condensed ice. However, it is clear that further investigations are required to verify this claim.

In this paper, we perform a follow-up study of Reinhardt et al. (2020) and investigate which SPH giant impact results can reproduce both the positive trend of the mass-distance distribution,

as well as the roughly 1 to 1 rock-to-ice ratio of Uranian regular satellites. We investigate only the oblique collisions with impact parameter $b \geq 0.6$, which have the potential to reproduce the large tilt and low internal heat flux of Uranus (Reinhardt et al., 2020; hereafter R20). Our study consists of three parts: SPH results (R20; Section 2.1), a 1D semi-analytical disc evolution model following Cilibrasi et al. (2018, 2021) to viciously evolve the disc (Section 2.2) and finally the GPU-based N-body simulations (Grimm and Stadel, 2014) to form the satellites from a disc of moonlets generated according to the results of the 1D semi-analytical disc evolution model (Section 2.3). Unlike Ida et al. (2020), we do not rely solely on analytical theory, but also on results from various numerical models to explain Uranus satellites formation. We also consider the rocky component of the impactor in order to compute the bulk composition of the satellites, which has not been done in the previous studies.

We present our results of the disc evolution model and N-body simulation in Section 3. We discuss the limitations and implications of our results in Section 4. We conclude our results in the final section.

2. Method

2.1. SPH simulations

As in R20 we use the SPH code Gasoline (Wadsley et al., 2004) with numerical improvements for planetary collisions (Reinhardt and Stadel, 2017; R20) to simulate the giant impacts. The particle representations of the planets prior to the impacts are obtained using ballistic (Reinhardt and Stadel, 2017; R20). R20 assumed a three layer structure (e.g. Nettelmann et al., 2013) for Uranus: a rocky core, an inner water and outer H-He envelope (see R20 for details). We re-simulated the most promising cases found in R20 with more realistic and thermodynamically consistent equations of state (EOS). We use ANEOS (Meier et al., 2021; Thompson and Lauson, 1974), a commonly-used EOS for impact simulations due to its large range of validity and the thermodynamically consistent treatment of phase transitions and phase mixtures (Benz et al., 1989), to model the heavy elements. For rock we use dunite (Benz et al., 1989) and water ice (Mordasini, 2020) for water. The H-He envelope is modelled as a linear mixture between H-REOS.3 and He-REOS.3 (Becker et al., 2014) with a He mass fraction of $Y=0.275$ using the additive volume law. Details on how the choice of EOS affects the impact outcome for given impact conditions can be found in Appendix A2.

In R20 an impact generated circumplanetary disc was considered a potential protosatellite disc if (i) it contains at least the total mass of Uranus' regular satellites in rock and ice, (ii) extends beyond the distance of Oberon and contains at least one Oberon mass ($\sim 3.5 \times 10^{-5} M_{\oplus}$) in rock and ice beyond this distance, and (iii) has a minimum rock mass of half the total current satellites' mass. Several of the impacts that substantially altered Uranus' tilt fulfill these requirements. Table 1 in the Appendix A1 shows the disc's parameters at the end of the SPH simulations that we consider in this study. In general, the total mass (including H-He, rock and water ice) of the impact generated discs shortly after the giant impact is one to two orders of magnitude more massive than the current Uranian satellites system ($\sim 10^{-4} M_{\oplus}$). The subsequent

viscous spreading of the disc would deplete $> 99\%$ of the disc mass, leaving the disc with the appropriate amount of rock and ice mass to form the satellite system.

2.2. 1D semi-analytical disc evolution

The SPH simulations provide the total H-He, ice, and rock mass that is ejected into the disc. We then study the disc's evolution by using a 1D semi-analytical approach, similar to the one already implemented for satellite population synthesis by Cilibrasi et al. (2018, 2021). First, we rely on the analytical solution of the 1D viscous disc equation (Pringle, 1981):

$$\frac{\partial \Sigma_g}{\partial t_{\text{disc}}} = \frac{1}{r} \frac{\partial}{\partial r} \left[3r^{1/2} \frac{\partial}{\partial r} (\Sigma_g \nu r^{1/2}) \right] \quad (1)$$

provided by Ida et al. (2020), where Σ_g is the surface density of the gas, $\nu = \alpha c_s^2 \Omega^{-1}$, where c_s is the sound's speed, Ω is the orbital frequency of the disc gas, and $\alpha = 10^{-3}$ is a constant parameter that represents the turbulence strength. At $t_{\text{disc}} = 0$, all the materials are supposed to be vapourized and distributed as:

$$\Sigma_g(r) = \Sigma_{g0} \left(\frac{r}{R_U} \right)^{-3/4} \exp \left[- \left(\frac{2r}{3r_{\text{disc}}} \right)^{5/4} \right], \quad (2)$$

where R_U is Uranus' radius and Σ_{g0} is chosen so that the total mass agrees with the value provided by the SPH simulations. r_{disc} is the mean radius of impact generated disc, taken from the SPH simulations and is defined as

$$r_{\text{disc}} = \left(\frac{J_{\text{disc}}/M_{\text{disc}}}{R_U^2 \Omega_U} \right)^2 R_U, \quad (3)$$

where J_{disc} is the total angular momentum of the disc, M_{disc} is the total mass of the disc, and Ω_U is the angular velocity of the disc at $r = R_U$ (Ida et al., 2020). This analytic solution agrees well with the surface density calculated from the SPH particles which in turn approximately follows a power-law with $\Sigma_g \sim r^{-3.25}$ similar to Ida et al. (2020). As in Ida et al. (2020) smaller differences will vanish during the later evolution due to viscous spreading of the disc and not affect our conclusions.

As long as a component (H-He, water or rock) is in the vapour state, its viscous evolution is computed following the analytical solution of Ida et al. (2020) (Eq. 1), including the temperature calculations. When the temperature reaches a value below 2000 K (Melosh, 2007), we assume that all the rock in that location condensed, and therefore the mass of rocks is shifted from the vapourised rock density profile to the solid rock density profile. This also occurs for the water when the temperature drops below 240 K (Ida et al., 2020), with vapourized water density profile being shifted to an ice density profile. We track a total of three vapour density profiles that follow an analytical evolution and two solid density profiles (rock and ice), which are evolved with a semi-analytical procedure that accounts for the interaction with the vapour.

To calculate the radial drift of the condensed solids, we first calculate the coupling between the condensed solid and vapour component via the Stokes number:

$$St = \frac{\pi a \rho_s}{2 \Sigma_g}, \quad (4)$$

where a is the size of the solid particles and ρ_s is their density. If the Stokes number approaches zero, the solid particles are well-coupled to the gas and evolve radially with the same analytical solution as in Eq. 1 and Eq. 2. If the Stokes number is high, the particles start to decouple from the gas and their radial speed is given by friction via

$$v_{r,\text{fric}} = H^2 \frac{St}{1+St^2} v_K, \quad (5)$$

where v_K is the Keplerian velocity, and $H \sim c_s/v_K$ is the aspect ratio of the disc. As expected, the radial velocity becomes zero when the solid particles get very large (together with St) and completely decouple from the gas. To consider both the radial velocities given by friction $v_{r,\text{fric}}$ and given by the analytical coupling with the gas $v_{r,\text{coup}}$, the total radial velocity of solids is set to be

$$v_r = v_{r,\text{fric}} + \frac{v_{r,\text{coup}}}{1+St^2} = \frac{H^2 St v_K + v_{r,\text{coup}}}{1+St^2}. \quad (6)$$

The surface density of the condensed solids are thus evolved based on v_r , which mainly depends on the St of the solid.

We perform semi-analytical simulations with the 1D disc evolution model for each set of parameters provided by SPH simulations (see Appendix A1 and Table 1) for 10,000 years, in order to generate the rock and ice surface density profiles to be used by the N-body simulations.

2.3. N-body simulations

We next apply the results at 10,000 years of the 1D disc evolution model (see the previous section) to generate the initial conditions of the moonlets for N-body simulations. We ensure that the disc has spread and cooled sufficiently so that moonlets can be formed when the solid (condensed ice and rock) to gas ratio of the local region is larger than one (Cilibrasi et al., 2018; Drażkowska and Dullemond, 2014). The solid surface density of the moonlets follows the surface density of the condensed ice and rock at 10,000 years computed from the 1D disc evolution model. Only regions beyond the synchronised radius of Uranus ($\sim 3.3 R_U$) are considered, since within the synchronised radius the satellite formed will be driven towards the planet by the tidal force.

The bulk density of the moonlets are computed based on the local condensed ice to rock ratio. We generate 20,000 equal mass moonlets for each simulation. The initial mass of each moonlet varies between each simulation, depending on the total mass of the condensed solids. The eccentricities and inclinations of the planetesimals are uniformly random in the range $0 < e < 0.01$ and $0^\circ < i < 0.5^\circ$. The nodal angles and mean anomalies of the moonlets are distributed randomly. We then perform the simulations with Uranus and a disc of planetesimals with the GPU-based N-body code *GENGA* (Grimm and Stadel, 2014), treating the full self-gravity between the moonlets. Simulations are performed for 5000 years with a timestep of 0.01 days. The gas disc is neglected since the H-He gas has depleted sufficiently at 10,000 years and thus the effect of Type-I migration on the moonlets is weak, as has been shown by Ida et al. (2020).

3. Results

We present the results of the most successful case which reproduces both the mass-distance distribution and the bulk composition of the satellites. The less successful cases are shown in Appendices A2--A4. We find that the characteristics of the current satellites are best reproduced by the following case:

- (1) a $3 M_{\text{Earth}}$ fully rocky impactor colliding with the proto-Uranus with $b = 0.75$ and $v_{\text{imp}} = 18.2 \text{ km s}^{-1}$;
- (2) condensed ice grows rapidly and decouples from the gas quickly ($St \rightarrow \infty$);
- (3) condensed rock remains micrometre size and couples well with the gas ($St \rightarrow 0$);
- (4) condensed rock sticks to the condensed ice in the same orbits.

Points (2) to (4) have been supported by the analytic theory of Ida et al. (2020) and the references therein, as icy particles are stickier than silicate particles (Blum and Wurm, 2008; Gundlach and Blum, 2014; Poppe et al., 2000).

The initial parameters of the disc are listed in Table 1 in Appendix A1 (Disc A2A). Fig. 1 shows the snapshots of Uranus and the impact generated disc from the SPH simulations 3.32 days after the impact. The total mass of the disc is $\sim 5 \times 10^{-2} M_{\odot}$, which is more than two orders of magnitude larger than the current satellite system's mass. The total mass of rock and ice comprises about half of the initial disc mass.

Right after the giant impact, the disc is hot and compact with about half of the disc's mass bounded within $r_{\text{disc}} = 2.55 R_{\text{U}}$ (the red circle on the left panel and the white circle on the right panel of Fig. 1). The temperature of most parts of the disc are nearly 10,000 K, implying that most of the rock and ice are still in vapour form. Different materials (shown as different colour SPH particles in Fig. 1) are homogeneously distributed throughout the disc, indicating that the disc is well mixed at this point in time.

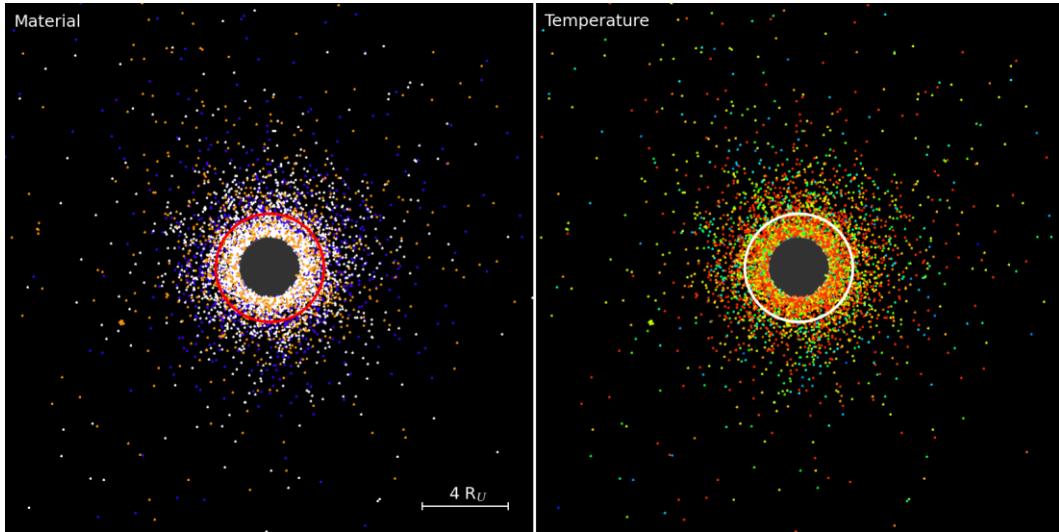


Fig. 1 - Snapshots of the impact generated disc from the SPH simulations 3.32 days after the impact (Disc A2A; Table 1). The left panel shows the material (rock: orange, ice: blue and H-He: white) and the right one temperature from 2×10^3 (blue) to 10^4 K (red). The size of one snapshot is $25 R_U$ (about the orbit of Umbriel). The red circle on the left panel and the white circle on the right panel show the mean disc radius $r_{\text{disc}} = 2.55 R_U$ within which about half of the disc mass is contained. The orbiting material consists of 5% of the total bound mass and is resolved with 5768 SPH particles. This disc is initially very hot ($T \sim 10,000$ K) and the different materials are well mixed and homogeneously distributed throughout the disc. All of the rock in orbit comes from the impactor.

3.1. Viscous spreading of the disc

Next, we evolve the impact generated disc with the 1D semi-analytical disc evolution model described in Section 2.2. Fig. 2 shows the time evolution of the surface density and the temperature of the impact generated disc. The initial surface density of the disc is modeled according to Eq. 2. At $t_{\text{disc}} = 0$ years, silicate particles (i.e. rock) condense beyond $\sim 7 R_U$ as the temperature beyond this distance falls below the silicate condensation temperature ($T_{\text{rock}} \sim 2000$ K; Melosh, 2007). Icy particles condense at distances beyond $\sim 15 R_U$ from Uranus due to the lower condensation temperature of water ($T_{\text{ice}} \sim 240$ K; Ida et al., 2020). Within a hundred years, the gas disc spreads beyond $100 R_U$ and the temperature of its inner region ($r < 20 R_U$) drops below T_{rock} , but remains higher than T_{ice} . Hence within $20 R_U$ only silicate particles condense but not the icy material. As silicate material remains small ($\sim 1 \mu\text{m}$), they couple well with the spreading gas ($St \rightarrow 0$) and thus adopt a similar surface density profile to the gas. The icy particles, on the other hand, remain in a similar surface density profile to the beginning as they grow quickly to km-sized moonlets and decoupled with the gas ($St \rightarrow \infty$).

From 100 to 1000 years, the gas surface density profile remains similar, but the disc continues to disperse and cool down. The temperature in between 8 to $20 R_U$ now also drops below the ice condensation temperature and thus leads to condensation of icy particles. Similar to the results from the analytical study of Ida et al. (2020), we observe a positive gradient for the surface density profile of the condensed ice starting to develop. Due to the continuous viscous spreading of the disc, gas, including uncondensed ice, in the innermost region falls onto Uranus by losing angular momentum. Therefore, the outer region of the disc is more enriched in icy material than the inner region (Ida et al., 2020).

From 1000 to 10,000 years, the ice condensation front continues to push inward as the temperature continues to drop. A positive surface density profile for the condensed ice has been developed from ~ 4 to $20 R_U$. The condensed silicate also follows a similar surface density profile because it is able to stick onto the condensed ice. This is ideal for generating a satellite system with bulk composition close to 1 to 1 in its rock-to-ice ratio.

Moving from the outer to the inner region of the disc, the silicate surface density starts deviating from the ice surface density profile at $\sim 7 R_U$ and eventually falls to zero at $\sim 4 R_U$ at $t_{\text{disc}} = 10,000$ years. This leaves the current Miranda region more ice dominated. This is caused by

the non-negligible gas drag acting on the micrometre size silicate particles. Hence, some of the condensed silicate particles are lost to Uranus due to the gas drag induced radial drift. We show in Section 3.3 that this is ideal for explaining the more icy composition and the lower mass of the innermost regular satellite Miranda.

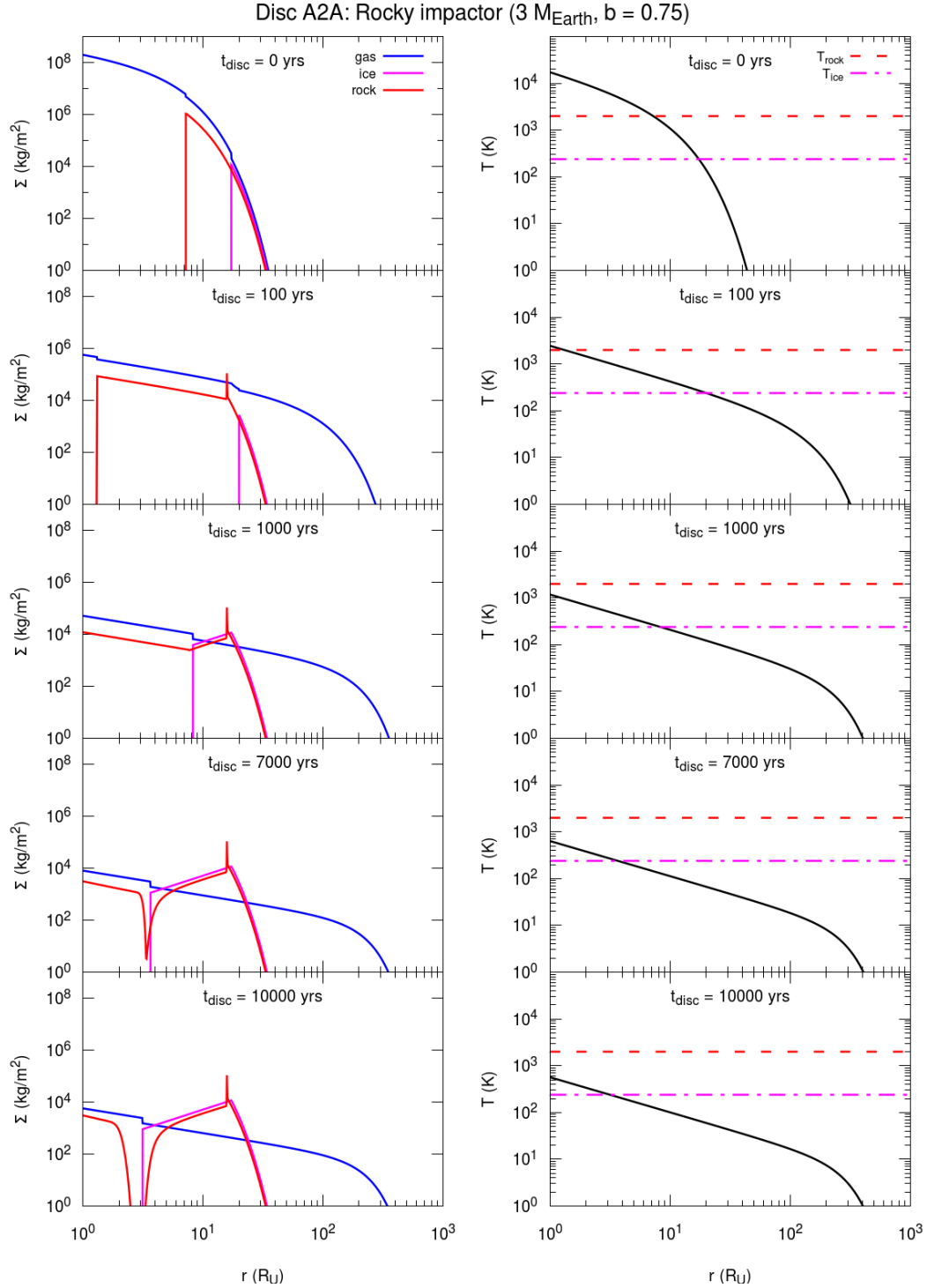


Fig. 2 - The left panel shows the evolution of the surface density of the gaseous component (blue), condensed ice (magenta) and condensed silicate (red) of the impact generated debris disc from $t_{\text{disc}} = 0$ to 10,000 years. The disc is generated by a fully rocky impactor colliding with proto-Uranus with $b = 0.75$ (Disc A2A of Table 1). The right panels depict the temperature profile of the disc, compared to the silicate condensation temperature (2000 K; red dashed line) and the water ice condensation temperature (240 K; magenta dashed-dotted line). At the end, the total condensed solids in the orbits ($6.3 \times 10^{-5} M_{\text{U}}$ of ice + $5.5 \times 10^{-5} M_{\text{U}}$ of silicate) follow a surface density profile with a positive gradient from ~ 4 to $20 R_{\text{U}}$ and the inner region ($4 R_{\text{U}} < r < 7 R_{\text{U}}$) is dominated by ice.

Disc A2A: Rocky impactor ($3 M_{\text{Earth}}$, $b = 0.75$)

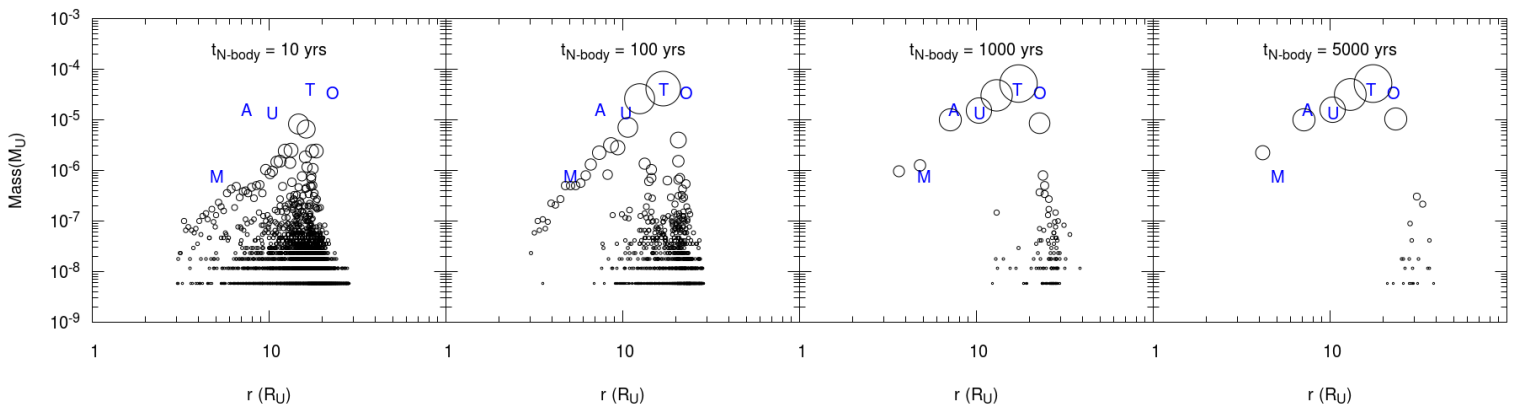


Fig. 3 - Growth of the satellites from a disc of equal mass moonlets in the N-body simulations from $t_{\text{N-body}} = 10$ to 5000 years. The initial condition of the moonlets follows the condensed solid surface density presented at $t_{\text{disc}} = 10,000$ years in Fig. 2 (Disc A2A of Table 1). The blue capital letters represent the current mass of the five regular Uranian satellites. The satellites we form, which have a total mass of $\sim 10^{-4} M_{\text{U}}$, follow a similar mass-distance distribution with the current system.

3.2. Growth of the satellites

Next, we generate a disc of moonlets based on the surface density profile of condensed solids at $t_{\text{disc}} = 10,000$ years as in Fig. 2 and perform the N-body simulation for 5,000 years to form a satellite system from the disc (as described in Section 2.3). Fig. 3 shows the mass evolution of the satellite system starting from a disc of equal mass moonlets. $t_{\text{N-body}} = 0$ years represents the formation time of the moonlet. As in Ishizawa et al. (2019) and Ida et al. (2020), we assume the moonlets form at the same time throughout the whole disc for simplicity. In reality, the outer region could begin forming moonlets earlier since it reaches a high solid to gas surface density earlier (see Fig. 2).

Due to a higher solid surface density in the outer region of the disc, more distant satellites grow more quickly and to larger size. Umbriel-sized objects ($\sim 10^{-5} M_{\text{U}}$) form within 10 years ($\sim 2,500$ orbits of Miranda) of the formation of the moonlets at $\sim 20 R_{\text{U}}$. Satellites with the mass of Titania (the largest satellite of Uranus) emerge within 100 years. At $t_{\text{N-body}} = 1,000$ years, nearly all the masses within $\sim 10 R_{\text{U}}$ are accreted by the Miranda, Ariel, and Umbriel analogues, while the outer region is still crowded with moonlets with masses less than Miranda's mass. These leftover moonlets are the residual of a decreased solid surface density beyond $20 R_{\text{U}}$ in Fig. 2, and they are slowly cleared by or accreted by the two outermost satellites in the current Titania and Oberon region from 1,000 to 5,000 years.

This particular case not only has the potential to reproduce the tilt and internal heat flux of Uranus, but also likely results in a satellite system comparable to the current system, in terms of the mass-distance distribution as well as the total number of the satellites. Similar to results of Ida et al. (2020), our simulation reproduces the current mass-distance distribution of the system, with the satellites' masses in general increasing with semi-major axis.

3.3. Bulk composition of the final system

In contrast to the previous studies on the formation of Uranus satellites (Ida et al., 2020; Ishizawa et al., 2019), we also consider the rocky component of the disc. Hence, we can study which impact cases lead to a satellite system with bulk compositions (i.e density) comparable to the current satellites. Our results indicate that a rocky impactor is required to reproduce the ~ 1 to 1 rock-to-ice ratio of the current system. After the giant impact, part of the target's and impactor's materials are ejected to form a circumplanetary disc. Since the mantle of Uranus is assumed to be water-rich (Helled et al., 2011; Nettelmann et al., 2013) in our SPH simulations, the impactor has to be rock-dominated in order to form a satellite system with a mixture of rock and ice. A large impact parameter collision ($b \geq 0.6$) is also required to generate Uranus tilt, which is a collision that cannot dredge up the silicate material deep in Uranus interior (if there are any).

Fig. 4 shows the final uncompressed density of the satellite system computed from our N-body simulation. Similar to the mass-distance distribution, there is a positive trend for the uncompressed density of the satellites, i.e. satellite density in general increases with orbital distances. According to Fig. 2, after $t_{\text{disc}} = 1,000$ years part of the silicate condensed in the inner region ($< 7 R_{\text{U}}$) are lost to Uranus through gas drag, while the outer region remains a constant ~ 1 to 1 condensed rock-to-ice ratio. This is because the silicate can stick onto the condensed ice and stay in their orbit in the outer region, whereas ice has not yet condensed in the inner region and silicates which feel the gas drag drift inward. As a result, the inner disc is more icy than the outer disc.

Based on the Voyager 2 measurements on masses and radii (Jacobson et al., 1992), the current satellites also show such a positive trend in their mean density. The blue data points in Fig. 4 represent the measured mean density of the satellites. The innermost satellite Miranda has the lowest mean density among the satellites, while the outermost large satellites Titania and Oberon could contain a higher mass fraction of rock than Miranda. Our model with condensed

silicate loss through gas drag in the inner disc could naturally explain the lower density of Miranda. Nevertheless, we emphasize that more accurate measurements on masses and radii of the Uranian satellites are required to confirm whether this density trend is robust.

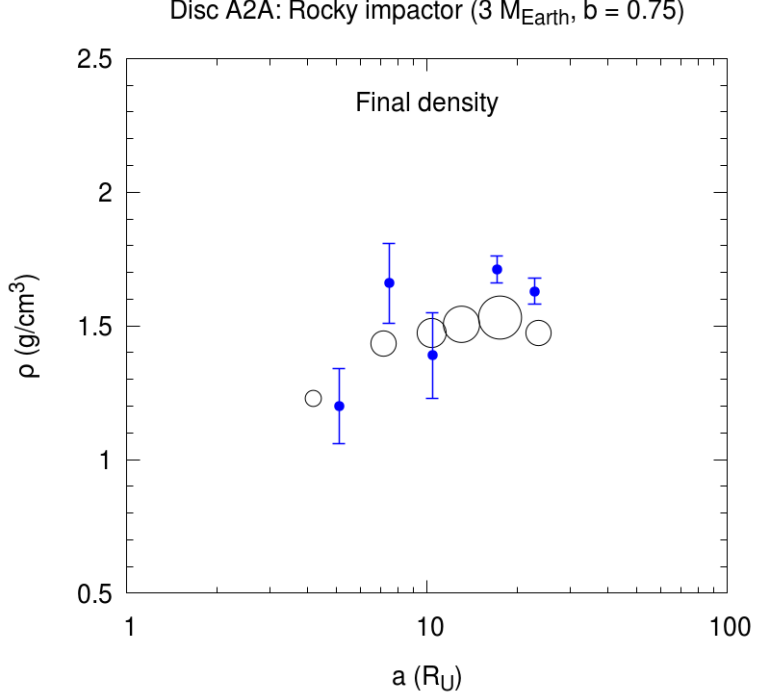


Fig. 4 - Uncompressed density of the final satellites at $t_{\text{N-body}} = 5,000$ years from the N-body simulations shown in Fig. 3 (Disc A2A of Table 1). The blue points and error bars represent the current density of the Uranus satellites taken from Jacobson et al. (1992). Only densities for objects with masses larger than $6 \times 10^{-7} M_{\text{U}}$ are shown. Note that our simulation reproduces the apparent positive trend of density, with the satellites' densities in general increasing with orbital distances in general.

4. Discussion

4.1. Investigation of failed cases

We also study the impact results other than those presented in the previous section. We find that changing the impactor composition from 100% rock to 50% ice and 50% rock results in a satellite system with a similar positive gradient mass-distance distribution, but the final system is too ice-rich (see Appendix A3 for details).

The assumptions on dust properties that we make in Section 3 affect the final system features. If we assume that both condensed silicate and icy particles stay at micrometre-size and do not stick together throughout the viscous spreading of the disc, then the final solid surface

density loses its positive gradient and hence cannot reproduce the mass-distance distribution of the current system (see Appendix A4 for details).

4.2. Uncertainties in Uranus' composition and the properties of its satellite system

The only spacecraft that has visited Uranus is *Voyager 2* in 1986. Due to the limited data our understanding of Uranus is very incomplete and there are still many uncertainties regarding this planet, including its exact bulk composition and internal structure (see reviews by Helled et al., 2020 and; Helled and Fortney, 2020 for discussion). It is often assumed, as in this study, that Uranus is mainly composed of water ice (~90 % of mass; Helled et al., 2011; Nettelmann et al., 2013), however, the actual abundance of water ice in Uranus is far from certain. A composition including ~82% of rock with the rest made of H-He can also match its observed properties (e.g. density, gravity field; Helled et al., 2011), although this is an extreme and improbable case. If Uranus contains a much higher amount of rock (e.g. ~50 % of mass) than most models have assumed, which can indeed be the case (Teanby et al., 2020), then the requirement of a rocky impact to generate the current satellite system could be relaxed. In such a case, the rocky component of the satellites can then also be delivered by the target of the collision.

We aim to reproduce the features of the current satellite system from our models. However, whether the Uranian system stays the same since its formation is still under debate. As suggested by the *Nice* model (Tsiganis et al., 2005), Uranus and Neptune could have undergone a phase of instability and inject huge amounts of Kuiper belt material into the inner solar system (e.g., Gomes et al., 2005; Mojzsis et al., 2019). It has been shown that this injected Kuiper belt material could also bombard the Uranian satellites, causing loss of volatiles, mass erosion and even catastrophic destruction of satellites (Nimmo and Korycansky, 2012; Wong et al., 2019). Hence, the Uranian system, prior to giant planet instability, could be more massive and ice rich. If that is the case, it would favor an impactor more enriched in ice (e.g. results in Appendix A2).

Given the short N-body simulation time, we neglect the tidal effect from Uranus on the satellite system. In principle, all satellites that form beyond the synchronous radius (~ 3 R_U) of Uranus would migrate outward through tidal interaction with Uranus and thus tidal evolution may play a role in shaping the final satellite system after its formation. It has been shown that the tidal migration of the satellites, which lead to their subsequent mutual mean-motion and secular resonance crossing, could explain the dynamical excitation of the system, in particular Mirada's relatively high inclination (Ćuk et al., 2020). However, according to analytical analysis satellites beyond ~7 R_U are unlikely to undergo sufficient migration that leads to mutual collision (Ishizawa et al., 2019). Besides, due to the uncertainty in Uranus' internal structure, the tidal quality factor Q of Uranus, which determines the migration rate of the satellites, is poorly constrained. Therefore, we neglect the effect of tides in the current discussion.

4.3. Rocky world beyond the ice line

Our results suggest that rocky objects could dominate the region beyond the ice line. We expect ice (including H_2O , CH_4 , NH_3) to rock condensate in a ratio of ~ 2 to 1 for solar composition gas (Lodders, 2003). However, some of the Kuiper objects have a rocky dominated composition. For example one of the largest Kuiper belt objects, Pluto, is likely to be 70% rock (McKinnon et al., 2017). Triton, which is the largest satellite of Neptune and likely captured from the Kuiper belt (Agnor and Hamilton, 2006; McCord, 1966; McKinnon, 1984), also consists of more than 70% of rock (McKinnon and Kirk, 2014). Combined with our results showing that a $\sim 3 M_{\text{Earth}}$ rock dominated impactor is required to form the satellites of Uranus, as well as the possibility of a more rocky Uranus (see previous subsection), all the evidences suggested that we may have to revise our picture of the formation of the outer solar system and gain a better understanding of how it could acquire such a rocky composition beyond the ice line.

5. Conclusions

The giant impact scenario remains the standard scenario to explain Uranus' properties (Kegerreis et al., 2018; Kurosaki and Inutsuka, 2018; Reinhardt et al., 2020) and the formation of its satellite system (Ida et al., 2020; Ishizawa et al., 2019). In this study, we revisited the SPH simulation results of the successful simulations of R20 to study which impact scenario best reproduces the satellite system of Uranus. By including new sets of SPH simulations with more advanced equation of state (Thompson and Lauson, 1974; Becker et al., 2014), followed by evolving the impact debris disc in a 1D disc evolution model (Cilibrasi et al., 2018, 2021), and growing the satellites from a disc of moonlets with N-body simulations (Grimm and Stadel, 2014), we found that the mass-distance distribution and the bulk composition of the satellites are best reproduced with a rocky impactor (100% rock) colliding with Uranus at $b = 0.75$ and $v_{\text{imp}} = 18.2 \text{ km s}^{-1}$. Such an oblique collision is also likely to explain the large tilt and the low internal heat flux of Uranus (R20). We also found that the assumption of dust properties are important. In order to reproduce the positive trend of the mass-distance distribution and the similar trend of the mean density of the system, condensed icy particles should grow quickly to decouple from the gas ($St \rightarrow \infty$), whereas the silicate particles should remain small ($St \rightarrow 0$) unless sticking to the condensed ice in the same orbit (Ida et al., 2020). The giant impact scenario can naturally explain the key features of Uranus and its regular moons. We therefore suggest that the Uranian satellite system formed as a result of an impact rather than from a circumplanetary disc.

While we can successfully reproduce the Uranian system, our model makes simplifying assumptions on the dust properties and neglects some detailed physical processes involved in dust condensation. For instance, we assume constant condensation temperatures for rock (2000 K) and ice (240 K). In reality, the condensation temperature of a material depends on the internal pressure of the gas, and the pressure changes when the disc spreads. We also neglect the release of latent heat when the solid condenses and this may change the temperature and pressure profile of the disc. Future studies should include detailed dust physics in studying the viscous spreading of the disc.

Our results also suggest that rocky objects could dominate the region beyond the ice line. However, we neglected several uncertainties regarding Uranus and its satellite system, including whether Uranus could have a more rocky bulk composition (Helled et al., 2011; Teanby et al., 2020) and whether the current Uranian system has remained unchanged since formation. The proposed *Nice* model instability of the giant planets (Tsiganis et al., 2005) could have a decisive impact on shaping the Uranian satellite system after formation (Nimmo and Korycansky, 2012; Wong et al., 2019). Future studies on Uranian satellite formation should also consider these uncertainties. Finally, we suggest that accurate measurements of the compositions, the tidal quality factor Q of Uranus and its regular moons with a future space mission (e.g. Fletcher et al., 2020) could constrain the origin and early evolution of Uranus and its satellite system. This in return will also shed light on the origin of our planetary system.

Acknowledgments

We would like to thank Thomas Meier and Jens Oppliger for their valuable contributions in implementing ANEOS and REOS3 for the SPH simulations presented in this paper. We would also like to thank Lucio Mayer and Judit Szulágyi for helpful discussions regarding the long term evolution of the proto-satellite disc. CR and RH thank Andreas Becker, Nadine Nettelmann, Yamila Miguel and Roland Redmer for fruitful discussions regarding the REOS3 equation of state. This work has been carried out within the framework of the National Center of Competence in Research PlanetS, supported by the Swiss National Science Foundation (SNSF). The authors acknowledge the financial support of the SNSF. The authors acknowledge the computational support from Service and Support for Science IT (S³IT) of University of Zurich and the Swiss National Supercomputing Centre (CSCS). RH acknowledges support from the Swiss National Science Foundation (SNSF) via grant 200020_188460.

Appendix A1. Disc parameters

We study the impact simulations from R20 that are most favorable in explaining Uranus' features and have the potential of forming the Uranian satellites based on the criteria set by R20. In addition, we perform extra sets of SPH simulation with the more advanced AENOS / REOS3 EOS. Table 1 shows the parameters of the impact generated disc from the SPH simulations that we investigated. In general, the impact generated disc has a total rock and ice mass at least an order of magnitude higher than the current satellite system. As we have shown in Section 3, both rock and ice are lost to Uranus through viscous spreading, causing less than 1% of rock and ice in the original disc to condense and eventually forming the moonlets of the system. Hence, an impactor of about $3 M_{\text{Earth}}$ ($0.206 M_{\text{U}}$) is required to form the satellite system with sufficient mass.

Table 1 - Parameters of the impact debris disc at the end of the SPH simulations (i.e. before vicious spreading). We model the proto-Uranus and the impactor with the Tillotson / ideal gas and ANEOS / REOS3 equation of state, respectively. In this table, we show the impactors' mass (M_{imp}), impactors' composition, impact parameter (b) and impact velocity (v_{imp}) of the collision, total mass of the impact generated disc (M_{disc}), total rock mass ($M_{\text{disc,rock}}$) and ice mass ($M_{\text{disc,ice}}$) in the disc, total angular momentum of the disc (J_{disc}) and the mean radius of the disc (r_{disc}). We highlight the most successful disc (A2A) in generating the current features of the Uranian satellite system.

	Disc	M_{imp} (M_{U})	Impactor composition	b	v_{imp} (km/s)	M_{disc} ($10^{-3}M_{\text{U}}$)	$M_{\text{disc,rock}}$ ($10^{-3}M_{\text{U}}$)	$M_{\text{disc,ice}}$ ($10^{-3}M_{\text{U}}$)	J_{disc} ($10^{15}\text{cm}^2\text{s}^{-1}$)	r_{disc} (R_{U})
Tillotson/ Ideal gas	A1T	0.138	100% rock	0.75	20.45	12.8	9.62	1.66	6.47	3.03
	A2T	0.206			20.53	44.8	22.6	8.46	6.01	2.61
	B1T	0.138	12% rock; 88% ice	0.65	19.48	7.28	0.03	6.49	6.98	3.52
	B2T	0.206			19.51	26.9	0.23	18.8	5.99	2.60
AENOS/ REOS3	A1A	0.138	100% rock	0.75	18.47	10.3	4.61	2.59	6.36	2.93
	A2A	0.206			18.20	49.9	9.21	15.1	5.94	2.55
	B1A	0.138	12% rock; 88% ice	0.65	17.90	2.89	0.00	2.06	6.34	2.91
	B2A	0.206			17.60	25.5	0.01	13.6	5.84	2.47
	CA	0.206	50% rock; 50% ice	0.60	17.81	26.4	0.06	12.2	5.82	2.45

	DA		27% rock; 73% ice		17.68	26.1	0.08	13.5	5.83	2.46
	EA		73% rock; 27% ice		17.96	24.9	0.32	8.35	5.82	2.45

Appendix A2. The Importance of a physically realistic EOS

In Section 3, we apply the AENOS / REOS3 EOS to model the internal structure of proto-Uranus and the impactor. We found that this yields slightly different results compared to the Tillotson / ideal gas models that R20 adopted. Fig. 5 shows the results of the disc evolution (left panel), mass (middle panel) and the uncompressed density (right panel) of the final satellites from the N-body simulation for the same impactor as described in Section 3, but with Uranus and the impactor modelled by the Tillotson / ideal gas EOS. Generally, we find that the total bound mass as well as the disc mass agree very well for both EOS combinations (see Table 1). However, in the case of the Tillotson / ideal gas EOS more rock originating from the impactor and less ice from proto-Uranus' inner envelope is ejected into orbit compared to the corresponding AENOS / REOS3 simulations. This is the result of the rocky impactor being more compact in case of AENOS, likely due to a more accurate treatment of the high pressure behaviour of rocks, which means that it is more difficult to be tidally disrupted and therefore less rock is deposited in the disk in the impact. The final satellite system generated by the Tillotson model is slightly more massive ($> 2 \times 10^{-4} M_{\text{U}}$; more than two times the current system) and is more rocky (ice to rock ratio ~ 0.3) than results of the AENOS model, even though the overall positive trend of the mass-distance distribution and the bulk density can still be reproduced.

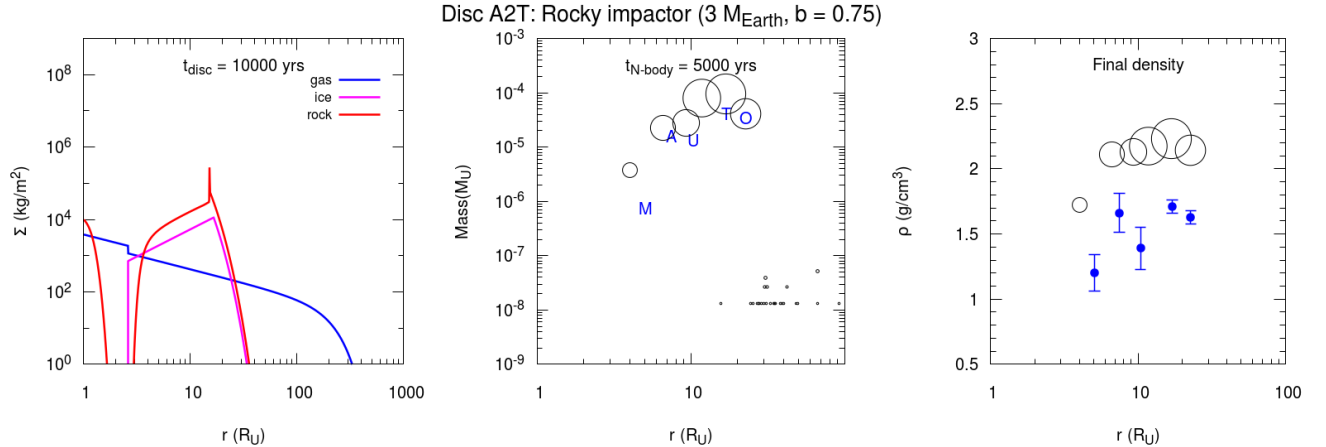


Fig. 5 - Results of the disc evolution (left panel), masses (middle panel) and the uncompressed density (right panel) of the final satellites from the N-body simulation. The disc is generated by the same impactor with the same b as the results shown in Section 3, but the proto-Uranus' and the impactor's internal structure is described by the Tillotson / ideal gas EOS (Disc A2T of Table 1). See Fig. 2, Fig. 3 and Fig. 4 for figures notation and colour description.

Appendix A3. Icy impactor results

Assuming a more icy impactor colliding with Uranus would lead to formation of a too icy satellite system. Fig. 6 shows the disc evolution and N-body simulation results after a $3 M_{\text{Earth}}$

impactor with 50% ice and 50% rock colliding with the proto-Uranus with $b = 0.6$ (Disc CA of Table 1). Similar to the results of a rocky impactor, after 10,000 years of disc spreading the condensed solid adopted a positive gradient of surface density profile from ~ 3 to $20 R_U$. However, different from Fig. 1, the solid surface density of condensed ice is roughly two orders of magnitude higher than the condensed silicate. This is because rock is enveloped by the icy mantle in the impactor, and thus the mass of rock ejected to the disc is two orders of magnitude lower in this case (Table 1). Even though the final N-body result follows a mass-distance distribution similar to the current system, the final system is too water-rich, with the satellites all having uncompressed density close to 1 g/cm^3 . Hence, compared to results presented in Section 3 for rocky impactor, results for an icy impactor are less successful. However, as discussed in Section 4.2., there are uncertainties regarding the internal composition of Uranus. If Uranus contains a higher fraction of rock (Helled et al., 2011; Teanby et al., 2020), it allows a more icy impactor to form the current satellites with their documented half-rock-half-ice composition.

Due to the limit of computational resources, we are only able to perform SPH simulation with $b = 0.6$ for the icy impactor. With a slightly larger b , similar to the successful case we presented in Section 3 ($b = 0.75$), we expect more rock could be ejected to disc. However, it is difficult to overcome a two order of magnitude difference between rock and ice mass by increasing b only. Hence, we expect the over-icy composition of the satellites obtained in this case would still persist even if the impact is slightly more oblique.

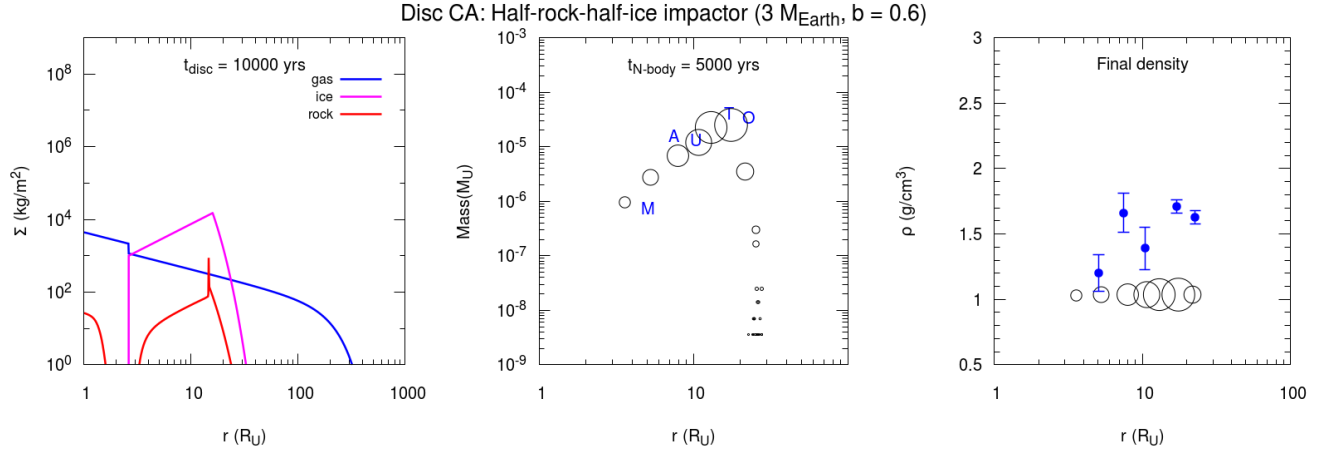


Fig. 6 - Same as Fig. 5, but for a half-rock-half ice impactor with a slightly lower impact parameter b (Disc CA of Table 1). The equation of state of the proto-Uranus is described by AENOS in this case.

Appendix A4. Changing the dust-gas interaction

The assumptions of the dust-gas interaction we made in Section 3 (point (2) to (4)) are also important in determining the final system. Fig. 7 depicts results for the same rocky impactor as in our successful case in Section 3, but assuming both condensed silicate and ice stay at micrometre size and silicates do not stick onto ice throughout the whole disc evolution.

Condensed solids at micrometre size couple well with the gas ($St \rightarrow 0$) and follow a solid surface density similar to gas surface density with negative gradient, although both rock and ice drift inward due to gas drag. A solid surface density with negative gradient has difficulty in forming Uranian satellites with their current mass-distance distribution since more condensed mass is concentrated in the region within $10 R_U$. Our N-body results indicate that instead of a few large satellites with masses in between 10^{-5} to $10^{-4} M_U$, we form more than 20 small satellites with masses roughly 10^{-7} to $10^{-6} M_U$. The total mass of the system is also an order of magnitude less massive than the current system, even though most of the satellites have a half-rock-half-ice composition. Hence, we conclude that the assumptions of the dust-gas interaction for rock and ice in Section 3 is crucial to successfully match the mass-distance distribution and bulk composition of the current Uranian satellite system.

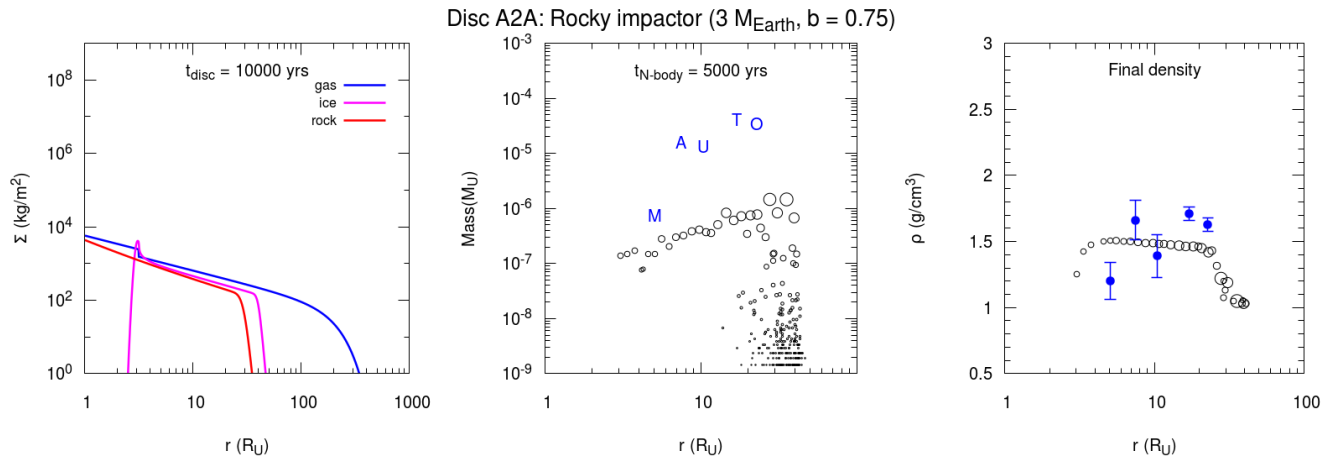


Fig. 7 - Same as Fig. 5, but assuming both condensed silicate and ice remain micrometre size ($St \rightarrow 0$) and evolve separately (i.e. silicate not sticking to ice) during the spreading of the disc. The equation of state of the proto-Uranus is described by AENOS in this case (Disc A2A of Table 1).

Reference

Agnor, C.B., Hamilton, D.P., 2006. Neptune's capture of its moon Triton in a binary–planet gravitational encounter. *Nature* 441, 192–194. <https://doi.org/10.1038/nature04792>

Becker, A., Lorenzen, W., Fortney, J.J., Nettelmann, N., Schöttler, M., Redmer, R., 2014. AB INITIO EQUATIONS OF STATE FOR HYDROGEN (H-REOS.3) AND HELIUM (He-REOS.3) AND THEIR IMPLICATIONS FOR THE INTERIOR OF BROWN DWARFS. *Astrophys. J. Suppl. Ser.* 215, 21. <https://doi.org/10.1088/0067-0049/215/2/21>

Benz, W., Cameron, A.G.W., Melosh, H.J., 1989. The origin of the Moon and the single-impact hypothesis III. *Icarus* 81, 113–131. [https://doi.org/10.1016/0019-1035\(89\)90129-2](https://doi.org/10.1016/0019-1035(89)90129-2)

Blum, J., Wurm, G., 2008. The Growth Mechanisms of Macroscopic Bodies in Protoplanetary Disks. *Annu. Rev. Astron. Astrophys.* 46, 21–56. <https://doi.org/10.1146/annurev.astro.46.060407.145152>

Canup, R.M., Ward, W.R., 2006. A common mass scaling for satellite systems of gaseous planets. *Nature* 441, 834–839. <https://doi.org/10.1038/nature04860>

Cilibrasi, M., Szulágyi, J., Grimm, S.L., Mayer, L., 2021. An N-body population synthesis framework for the formation of moons around Jupiter-like planets. *Mon. Not. R. Astron. Soc.*

Soc. <https://doi.org/10.1093/mnras/stab1179>

Cilibrasi, M., Szulágyi, J., Mayer, L., Drążkowska, J., Miguel, Y., Inderbitzi, P., 2018. Satellites form fast & late: a population synthesis for the Galilean moons. *Mon. Not. R. Astron. Soc.* 480, 4355–4368. <https://doi.org/10.1093/mnras/sty2163>

Ćuk, M., Moutamid, M.E., Tiscareno, M.S., 2020. Dynamical History of the Uranian System. *Planet. Sci. J.* 1, 22. <https://doi.org/10.3847/PSJ/ab9748>

Drążkowska, J., Dullemond, C.P., 2014. Can dust coagulation trigger streaming instability? *Astron. Astrophys.* 572, A78. <https://doi.org/10.1051/0004-6361/201424809>

Fletcher, L.N., Helled, R., Roussos, E., Jones, G., Charnoz, S., André, N., Andrews, D., Bannister, M., Bunce, E., Cavelié, T., Ferri, F., Fortney, J., Grassi, D., Griton, L., Hartogh, P., Hueso, R., Kaspi, Y., Lamy, L., Masters, A., Melin, H., Moses, J., Mousis, O., Nettleman, N., Plainaki, C., Schmidt, J., Simon, A., Tobie, G., Tortora, P., Tosi, F., Turrini, D., 2020. Ice Giant Systems: The scientific potential of orbital missions to Uranus and Neptune. *Planet. Space Sci.* 191, 105030. <https://doi.org/10.1016/j.pss.2020.105030>

Fortney, J.J., Ikoma, M., Nettelmann, N., Guillot, T., Marley, M.S., 2011. SELF-CONSISTENT MODEL ATMOSPHERES AND THE COOLING OF THE SOLAR SYSTEM\textquotesingle GIANT PLANETS. *Astrophys. J.* 729, 32. <https://doi.org/10.1088/0004-637X/729/1/32>

Gomes, R., Levison, H.F., Tsiganis, K., Morbidelli, A., 2005. Origin of the cataclysmic Late Heavy Bombardment period of the terrestrial planets. *Nature* 435, 466–469. <https://doi.org/10.1038/nature03676>

Grimm, S.L., Stadel, J.G., 2014. THE GENGA CODE: GRAVITATIONAL ENCOUNTERS INN-BODY SIMULATIONS WITH GPU ACCELERATION. *Astrophys. J.* 796, 23. <https://doi.org/10.1088/0004-637X/796/1/23>

Gundlach, B., Blum, J., 2014. THE STICKINESS OF MICROMETER-SIZED WATER-ICE PARTICLES. *Astrophys. J.* 798, 34. <https://doi.org/10.1088/0004-637X/798/1/34>

Hartmann, L., Calvet, N., Gullbring, E., D\textquotesingle Alessio, P., 1998. Accretion and the Evolution of T Tauri Disks. *Astrophys. J.* 495, 385–400. <https://doi.org/10.1086/305277>

Helled, R., Anderson, J.D., Podolak, M., Schubert, G., 2011. INTERIOR MODELS OF URANUS AND NEPTUNE. *Astrophys. J.* 726, 15. <https://doi.org/10.1088/0004-637X/726/1/15>

Helled, R., Fortney, J.J., 2020. The interiors of Uranus and Neptune: current understanding and open questions. *Philos. Trans. R. Soc. Math. Phys. Eng. Sci.* 378, 20190474. <https://doi.org/10.1098/rsta.2019.0474>

Helled, R., Nettelmann, N., Guillot, T., 2020. Uranus and Neptune: Origin, Evolution and Internal Structure. *Space Sci. Rev.* 216, 38. <https://doi.org/10.1007/s11214-020-00660-3>

Ida, S., Ueta, S., Sasaki, T., Ishizawa, Y., 2020. Uranian satellite formation by evolution of a water vapour disk generated by a giant impact. *Nat. Astron.* 4, 880–885. <https://doi.org/10.1038/s41550-020-1049-8>

Ishizawa, Y., Sasaki, T., Hosono, N., 2019. Can the Uranian Satellites Form from a Debris Disk Generated by a Giant Impact? *Astrophys. J.* 885, 132. <https://doi.org/10.3847/1538-4357/ab48ef>

Jacobson, R.A., Campbell, J.K., Taylor, A.H., Synnott, S.P., 1992. The masses of Uranus and its major satellites from Voyager tracking data and earth-based Uranian satellite data. *Astron. J.* 103, 2068–2078. <https://doi.org/10.1086/116211>

Kegerreis, J.A., Teodoro, L.F.A., Eke, V.R., Massey, R.J., Catling, D.C., Fryer, C.L., Korycansky, D.G., Warren, M.S., Zahnle, K.J., 2018. Consequences of Giant Impacts on Early Uranus for Rotation, Internal Structure, Debris, and Atmospheric Erosion. *Astrophys. J.* 861, 52. <https://doi.org/10.3847/1538-4357/aac725>

Kurosaki, K., Inutsuka, S., 2018. The Exchange of Mass and Angular Momentum in the Impact Event of Ice Giant Planets: Implications for the Origin of Uranus. *Astron. J.* 157, 13. <https://doi.org/10.3847/1538-3881/aaf165>

Lodders, K., 2003. Solar System Abundances and Condensation Temperatures of the Elements. *Astrophys. J.* 591, 1220–1247. <https://doi.org/10.1086/375492>

McCord, T.B., 1966. Dynamical evolution of the Neptunian system. *Astron. J.* 71, 585. <https://doi.org/10.1086/109967>

McKinnon, W.B., 1984. On the origin of Triton and Pluto. *Nature* 311, 355–358. <https://doi.org/10.1038/311355a0>

McKinnon, W.B., Kirk, R.L., 2014. Chapter 40 - Triton, in: Spohn, T., Breuer, D., Johnson, T.V. (Eds.), *Encyclopedia of the Solar System (Third Edition)*. Elsevier, Boston, pp. 861–881. <https://doi.org/10.1016/B978-0-12-415845-0.00040-2>

McKinnon, W.B., Stern, S.A., Weaver, H.A., Nimmo, F., Bierson, C.J., Grundy, W.M., Cook, J.C., Cruikshank, D.P., Parker, A.H., Moore, J.M., Spencer, J.R., Young, L.A., Olkin, C.B., Ennico Smith, K., 2017. Origin of the Pluto–Charon system: Constraints from the New Horizons flyby. *Icarus*, Special Issue: The Pluto System 287, 2–11. <https://doi.org/10.1016/j.icarus.2016.11.019>

Meier, T., Reinhardt, C., Stadel, J.G., 2021. The EOS/Resolution Conspiracy: Convergence in Proto-Planetary Collision Simulations. *Mon. Not. R. Astron. Soc.* <https://doi.org/10.1093/mnras/stab1441>

Melosh, H.J., 2007. A hydrocode equation of state for SiO₂. *Meteorit. Planet. Sci.* 42, 2079–2098. <https://doi.org/10.1111/j.1945-5100.2007.tb01009.x>

Mojzsis, S.J., Brasser, R., Kelly, N.M., Abramov, O., Werner, S.C., 2019. Onset of Giant Planet Migration before 4480 Million Years Ago. *Astrophys. J.* 881, 44. <https://doi.org/10.3847/1538-4357/ab2c03>

Mordasini, C., 2020. Planetary evolution with atmospheric photoevaporation - I. Analytical derivation and numerical study of the evaporation valley and transition from super-Earths to sub-Neptunes. *Astron. Astrophys.* 638, A52. <https://doi.org/10.1051/0004-6361/201935541>

Mosqueira, I., Estrada, P.R., 2003. Formation of the regular satellites of giant planets in an extended gaseous nebula I: subnebula model and accretion of satellites. *Icarus* 163, 198–231. [https://doi.org/10.1016/S0019-1035\(03\)00076-9](https://doi.org/10.1016/S0019-1035(03)00076-9)

Nettelmann, N., Helled, R., Fortney, J.J., Redmer, R., 2013. New indication for a dichotomy in the interior structure of Uranus and Neptune from the application of modified shape and rotation data. *Planet. Space Sci., Surfaces, atmospheres and magnetospheres of the outer planets and their satellites and ring systems: Part VIII* 77, 143–151. <https://doi.org/10.1016/j.pss.2012.06.019>

Nimmo, F., Korycansky, D.G., 2012. Impact-driven ice loss in outer Solar System satellites: Consequences for the Late Heavy Bombardment. *Icarus* 219, 508–510. <https://doi.org/10.1016/j.icarus.2012.01.016>

Pearl, J.C., Conrath, B.J., 1991. The albedo, effective temperature, and energy balance of Neptune, as determined from Voyager data. *J. Geophys. Res. Space Phys.* 96, 18921–18930. <https://doi.org/10.1029/91JA01087>

Poppe, T., Blum, J., Henning, T., 2000. Analogous Experiments on the Stickiness of Micron-sized Preplanetary Dust. *Astrophys. J.* 533, 454–471. <https://doi.org/10.1086/308626>

Pringle, J.E., 1981. Accretion Discs in Astrophysics. *Annu. Rev. Astron. Astrophys.* 19, 137–160. <https://doi.org/10.1146/annurev.aa.19.090181.001033>

Reinhardt, C., Chau, A., Stadel, J., Helled, R., 2020. Bifurcation in the history of Uranus and Neptune: the role of giant impacts. *Mon. Not. R. Astron. Soc.* 492, 5336–5353. <https://doi.org/10.1093/mnras/stz3271>

Reinhardt, C., Stadel, J., 2017. Numerical aspects of giant impact simulations. *Mon. Not. R. Astron. Soc.* 467, 4252–4263. <https://doi.org/10.1093/mnras/stx322>

Safronov, V.S., 1966. Sizes of the largest bodies falling onto the planets during their formation. *Sov. Astron.* 9, 987–991.

Slattery, W.L., Benz, W., Cameron, A.G.W., 1992. Giant impacts on a primitive Uranus. *Icarus* 99, 167–174. [https://doi.org/10.1016/0019-1035\(92\)90180-F](https://doi.org/10.1016/0019-1035(92)90180-F)

Szulágyi, J., Ciliberti, M., Mayer, L., 2018. In Situ Formation of Icy Moons of Uranus and Neptune. *Astrophys. J.* 868, L13. <https://doi.org/10.3847/2041-8213/aaeed6>

Teanby, N.A., Irwin, P.G.J., Moses, J.I., Helled, R., 2020. Neptune and Uranus: ice or rock giants? *Philos. Trans. R. Soc. Math. Phys. Eng. Sci.* 378, 20190489. <https://doi.org/10.1098/rsta.2019.0489>

Thompson, S.L., Lauzon, H.S., 1974. Improvements in the CHART D radiation-hydrodynamic code III: revised analytic equations of state (No. SC-RR-71-0714). Sandia Labs., Albuquerque, N.Mex. (USA).

Tsiganis, K., Gomes, R., Morbidelli, A., Levison, H.F., 2005. Origin of the orbital architecture of the giant planets of the Solar System. *Nature* 435, 459–461. <https://doi.org/10.1038/nature03539>

Wadsley, J.W., Stadel, J., Quinn, T., 2004. Gasoline: a flexible, parallel implementation of TreeSPH. *New Astron.* 9, 137–158. <https://doi.org/10.1016/j.newast.2003.08.004>

Wong, E.W., Brasser, R., Werner, S.C., 2019. Impact bombardment on the regular satellites of Jupiter and Uranus during an episode of giant planet migration. *Earth Planet. Sci. Lett.* 506, 407–416. <https://doi.org/10.1016/j.epsl.2018.11.023>